Pis'ma v ZhETF, vol. 102, iss. 1, pp. 3 – 9 

# System of neutron microbeams from a planar waveguide

*S. V. Kozhevnikov*[+1)], *V. K. Ignatovich*[+], *Yu. V. Nikitenko*[+], *F. Ott*[*×], *A. V. Petrenko*[+]

[+]*Frank Laboratory of Neutron Physics, Joint Institute for Nuclear Research, 141980 Dubna, Russia*

[*]*CEA, IRAMIS, Laboratoire Léon Brillouin, F-91191 Gif sur Yvette, France*

[×]*CNRS, IRAMIS, Laboratoire Léon Brillouin, F-91191 Gif sur Yvette, France*

Submitted 28 April 2015
Resubmitted 25 May 2015

Results of experimental investigations of space, angular and wavelength distribution in neutron microbeams obtained for the first time with the help of a resonant planar neutron waveguide at the time-of-flight reflectometer of the IBR-2 pulsed reactor are reported and comparison with theoretical calculations is presented. Possible application of microbeams in physical experiments is discussed.

DOI: 10.7868/S0370274X15130019

**1. Introduction.** Neutron scattering is a powerful tool for investigations of magnetic and nonmagnetic solids, polymers and biological objects. Results of experiments depend on properties of the incident neutron beam: its collimation, monochromatization and size. The commonly used beams have the width of the order of 0.1–10 mm. For local investigation of samples the more narrow beams are required. The various focusing devices [1] are able to decrease the width of the neutron beam up to 50 $\mu$m. The smaller widths up to $0.1-10\,\mu$m can be achieved with the help of planar waveguides, which transform collimated neutron macrobeams into slightly divergent microbeams compressed in one dimension. Production of such microbeams of nonpolarized neutrons is reported in [2, 3]. A polarized microbeam was reported in [4]. A combination of nonmagnetic neutron waveguide with polarized neutron reflectometer [5] was used for investigations of an amorphous magnetic microwire [6, 7] by the method of spin precession at transmission [8]. All the previous experiments with microbeams were made at steady state reactors with monochromatic incident neutron beams. A monochromatic neutron beam, incident at a fixed grazing angle on a planar resonant waveguide, produces only a single microbeam.

In the present communication, we report experimental results obtained at a time-of-flight (TOF) reflectometer. In this case at a given grazing angle of an incident beam several microbeams can be observed simultaneously. It gives an opportunity to investigate properties of the microbeams in more details. We measured their space, angular and wavelength distribution. Compare their angular divergence with predictions of Fraunhofer diffraction at the exit slit of a planar waveguide.

In the next section the experimental setup is described, in the third section experimental results are reported, in the fourth section angular distribution of the obtained microbeams were compared with the prediction of theory of the Fraunhofer diffraction, in the fifth section a comparison of experiments with micro beams at steady state and pulsed neutron sources is given and in the last section after a summary the possible application of microbeams is discussed.

**2. Experimental setup.** The experiment was done at the polarized neutron time-of-flight reflectometer REMUR [9] of the pulsed reactor IBR-2 (FLNP, JINR, Dubna, Russia). The incident neutron beam was extracted directly from the thermal moderator or from the moderator with the cold source supplement. The beam from the thermal moderator without cold source contained 3 times more neutrons within wavelengths range 1–3 Å, but the moderator with the cold source [10] produced 10 times more neutrons with wavelengths in the interval 3–8 Å. The maximal neutron wavelength of neutron spectra extracted from thermal and cold moderators was 8 and 16 Å, respectively.

The scheme of the experiment is shown in Fig. 1a. The resonant planar waveguide is a multilayer $Ni_{67}Cu_{33}/Cu/Ni_{67}Cu_{33}//Si$(substrate) with optical nuclear potential shown in Fig. 1b. At room temperature the alloy Ni(67 % at.)Cu(33 % at.) is nonmagnetic. The initial neutron beam falls onto the sample surface under a grazing angle $\theta_i$, and tunnels through the upper layer into the wave guiding layer (channel) made

[1)]e-mail: kozhevn@nf.jinr.ru

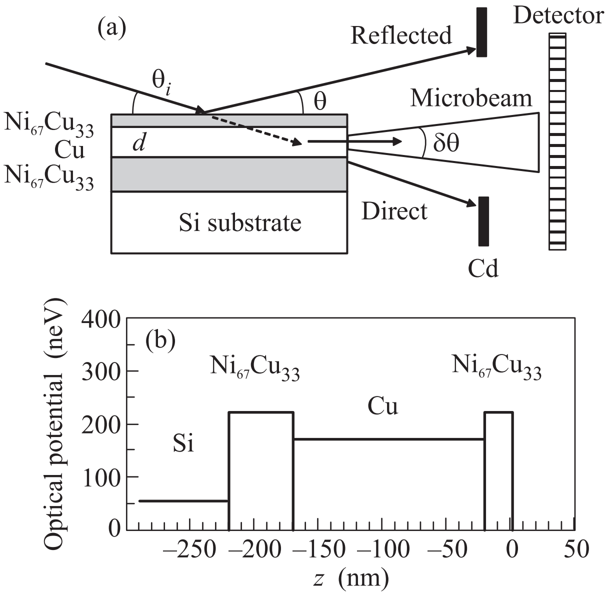


Fig. 1. (a) – Scheme of experiment. (b) – Neutron optical potential of the sample as a function of the coordinate $z$ perpendicular to the sample layers

of Cu. Inside the middle layer the neutron wave density at some wavelengths is resonantly enhanced [11]. In the potential system Fig. 1b three resonances of orders $n = 0, 1, 2$ correspond to the region of total reflection of the neutrons from the bottom layer $Ni_{67}Cu_{33}$. There are also resonances with $n > 2$ but their intensity is lower because neutrons at these resonances can pass through the bottom layer $Ni_{67}Cu_{33}$ outside the waveguide. The enhanced neutron wave after channeling [12–14] along the guiding layer reaches the exit edge and leaks out through the gap of the width $d$ equal to the thickness of the channeling layer. The outgoing microbeam has an angular divergence $\delta\theta$, which is determined by the law of the Fraunhofer diffraction

$$\delta\theta \sim \lambda/d, \qquad (1)$$

where $\lambda$ is the neutron wavelength. The divergent microbeam is registered by two-dimensional position-sensitive (PSD) $^3$He detector with spatial resolution 2.7 mm. The distance sample-detector was 4.94 m. The full time-of-flight base was 33.94 m. The angular divergence of the incident beam was 1.2 mrad.

**3. Experimental results.** The parameters of the sample found in a neutron reflectometry measurements were $CuO(2.5\,nm)/Ni_{67}Cu_{33}(14.9)/Cu(141.7)/Ni_{67}Cu_{33}(53.3)//$ Si(substrate). These measured layer thicknesses were used in calculations. The nuclear potentials were found to be: CuO (45 neV), upper layer $Ni_{67}Cu_{33}$ (245 neV), Cu (171 neV), bottom layer $Ni_{67}Cu_{33}$ (219 neV), Si (54 neV).

With time-of-flight technique it is possible to obtain at PSD a two-dimensional map of neutron counts for any grazing angle of the incident beam. One such a map for the grazing angle $\theta_i = 7.68$ mrad of the incident beam is presented in Fig. 2. The horizontal axis corresponds to

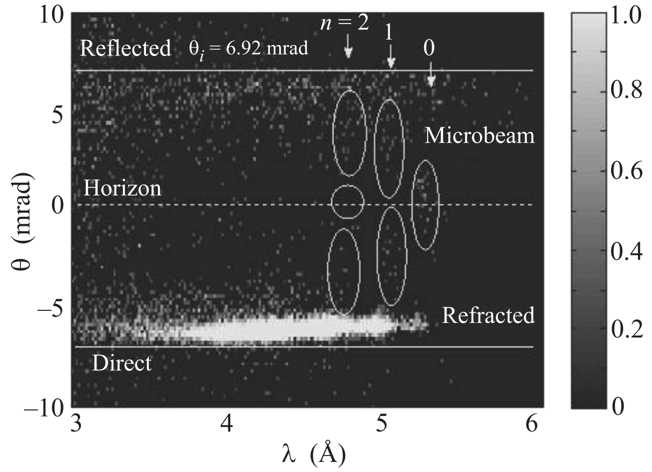


Fig. 2. Two-dimensional map of the neutron intensity in dependence on the neutron wavelength and the scattering angle at the fixed grazing angle of the incident beam 7.68 mrad. The ovals show the calculated positions of the microbeams of different orders. The points around them are related to background created by scattering and also to refracted and specularly reflected parts of the incident beam

neutron wavelength $\lambda$ and the vertical one corresponds to the outgoing with respect to horizon angle $\theta$. The specularly reflected and direct beams were blocked by Cd beam-stops as shown in Fig. 1a. The counts near position of the direct beam correspond to the refracted one. The spots marked by ellipses correspond to the microbeams of different resonance orders $n = 0, 1, 2$. The space distribution of the neutron microbeam intensity reflects the two-dimensional distribution of the neutron wave function density $|\psi_n(z, \lambda)|^2$ in the waveguide [3], where $z$ is the coordinate perpendicular to the sample surface and $n = 0, 1, 2, ...$ is the resonance order. The two-dimensional map represents the distributed low intensity of the microbeams comparable to the level of background. It is difficult to see well-defined spots of the beams in this case. But we can see the peaks on the integrated intensity.

In Fig. 3, the dependence of the neutron intensity registered by PSD on the neutron wavelength is shown for various grazing angles of the incident beam. The intensity was integrated over the wide angle range be-

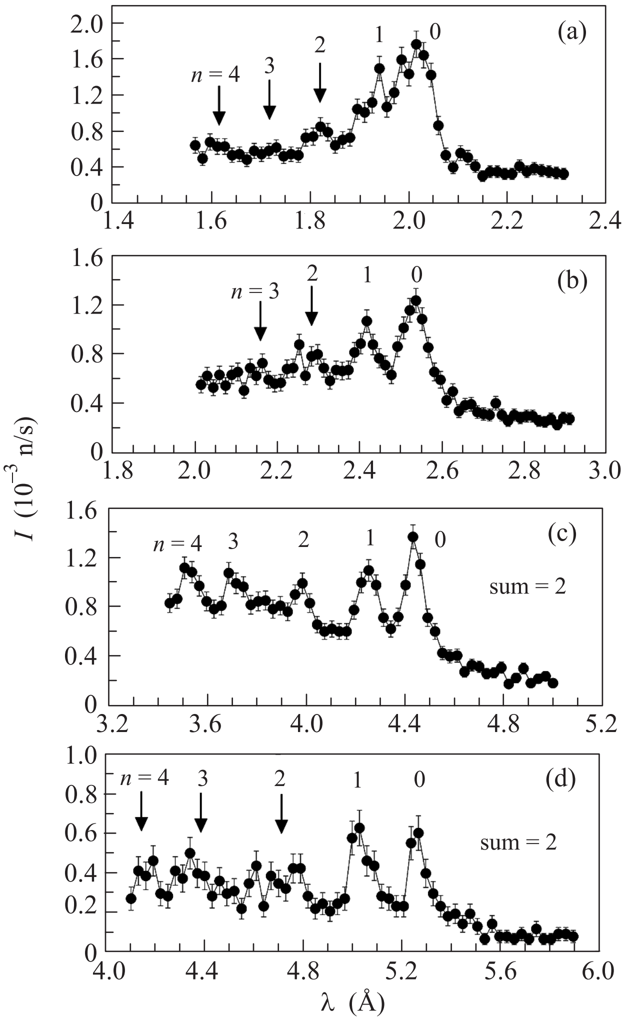


Fig. 3. The neutron intensity as a function of the neutron wavelength at various grazing angles of the incident beam: 2.93 (a), 3.63 (b), 6.46 (c), 7.68 (d) mrad. The energy at the resonances $n = 0$, 1, 2 correspond to total reflection of neutrons from the bottom $Ni_{67}Cu_{33}$ thick layer. The microbeam intensity is higher. The neutron microbeam intensity of the resonances $n > 2$ is lower because of the neutron transmission through the bottom $Ni_{67}Cu_{33}$ thick layer

tween specularly reflected and the direct beams. Measurements at $\theta_i = 2.93$ mrad were made without cold source, and measurements at other grazing angles of the incident beam were done with the cold source at the thermal moderator. The maxima of the neutron counts correspond to various resonance orders. The neutron wavelength of a microbeam decreases with decrease of the grazing angle of the incident beam and with increase of the resonance order. At the angles 3.63, 6.46, and 7.68 mrad the presented intensity is summed over two nearby wavelength channels to diminish the statistical error bar.

In Fig. 4 the dependence of microbeams neutron intensity on exit angle is shown for various resonance or-

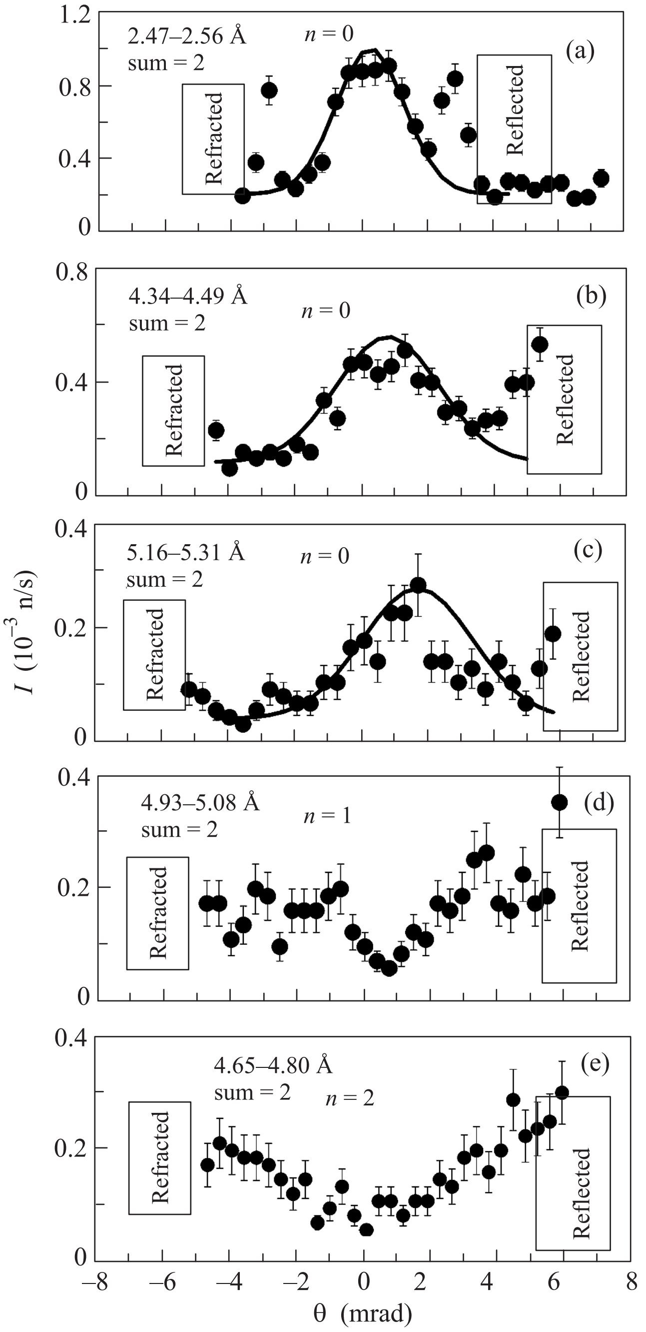


Fig. 4. The neutron intensity as a function of the grazing angle of the scattered beam for different resonance orders at various grazing angles of the incident beam: 3.63 mrad, $n = 0$ (a); 6.46 mrad, $n = 0$ (b); 7.68 mrad, $n = 0$ (c); 7.68 mrad, $n = 1$ (d); 7.68 mrad, $n = 2$ (e)

ders and grazing angles of the incident beam. Figs. 4a–c correspond to the resonance order $n = 0$ and grazing angles of the incident beam equal to 3.63, 6.46, and

7.68 mrad respectively. Left (refracted) and right (specularly reflected) beam regions around the microbeam peaks are blocked by Cd beam-stops to diminish the background level. It is clearly seen that the width of the central peak increases with increase of the neutron wavelength as follows from Fraunhofer diffraction theory. Quantitative description of the experimental data with the theory will be presented in the next section.

Figs. 4c–e correspond to grazing angle of the incident beam $\theta_i = 7.68$ mrad and to the resonance orders $n = 0$, 1, 2, respectively. The neutron intensity of the microbeam has one, two, and three maxima for the resonances $n = 0$, 1, 2, respectively [2, 3]. The experimental data are well described by the theory. Our experimental data show one peak for the resonance $n = 0$ (Fig. 4c) with maximum at $\theta = +1$ mrad and two peaks for the resonance $n = 1$ (Fig. 4d) with maxima at $\theta = -2$ mrad and $\theta = +4$ mrad. The asymmetry means that the horizontal direction in our measurements must be shifted to the angle $\theta = +1$ mrad.

At the resonance $n = 2$ (Fig. 4e), the intensity increases toward the left and right sides and is partly cut off by the beam-stops. The angular distributions of the neutron intensity shown in Figs. 4c–e are qualitatively in agreement with the results of [2, 3, 15]. The angular positions of microbeam peaks maxima of the resonances $n = 0$, 1, 2 can be measured separately simultaneously, because with the time-of-flight technique they are shifted in wavelength.

In the reference [15], we have registered the neutron microbeams from the same sample CuO(2.5 nm)/$Ni_{67}Cu_{33}$(14.9)/Cu(141.7)/$Ni_{67}Cu_{33}$(53.3)// Si(substrate) at the neutron reflectometer NREX (reactor FRM II, Garching, Germany) using fixed neutron wavelength 4.26 Å (1 % FWHM). The angular divergence of the incident beam was 0.1 mrad and the angular resolution of the two-dimensional $^3$He position-sensitive detector was 1.0 mrad. In Fig. 5a, the two-dimensional map of neutron intensity in the coordinates $(\theta_i, \theta)$ is shown. The ovals mark the positions of the neutron microbeams of the resonances $n = 0$, 1, 2. One can see more clearly the spots of the microbeams because of the better statistics and low background. The neutron microbeam intensity was integrated over the scattering angles in the region between two diagonal lines. In Fig. 5b, the integrated microbeam intensity is presented as a function of the grazing angle of the incident beam. Three peaks of the resonances $n = 0$, 1, 2 are well defined. In Fig. 5c, the microbeam intensity integrated in the region of the angles $\theta_i$ over the resonances width is shown as a function of the diffraction angle $\theta$. One can see one maximum for the resonance $n = 0$, two maxima at $\theta = \pm 2$ mrad for the resonance $n = 1$ and three maxima for the resonance $n = 2$ (two maxima at $\theta = \pm 3$ mrad and low maximum in the center around $\theta = 0$ mrad). Comparing data of the resonances $n = 0$, 1, 2, one can conclude that the perpendicular to the sample surface wave vector $k_{\perp n} = 2\pi\theta_i/\lambda_n$ at the time-of-flight method coincides with $k_{\perp n} = 2\pi\theta_{in}/\lambda$ at the fixed wavelength technique.

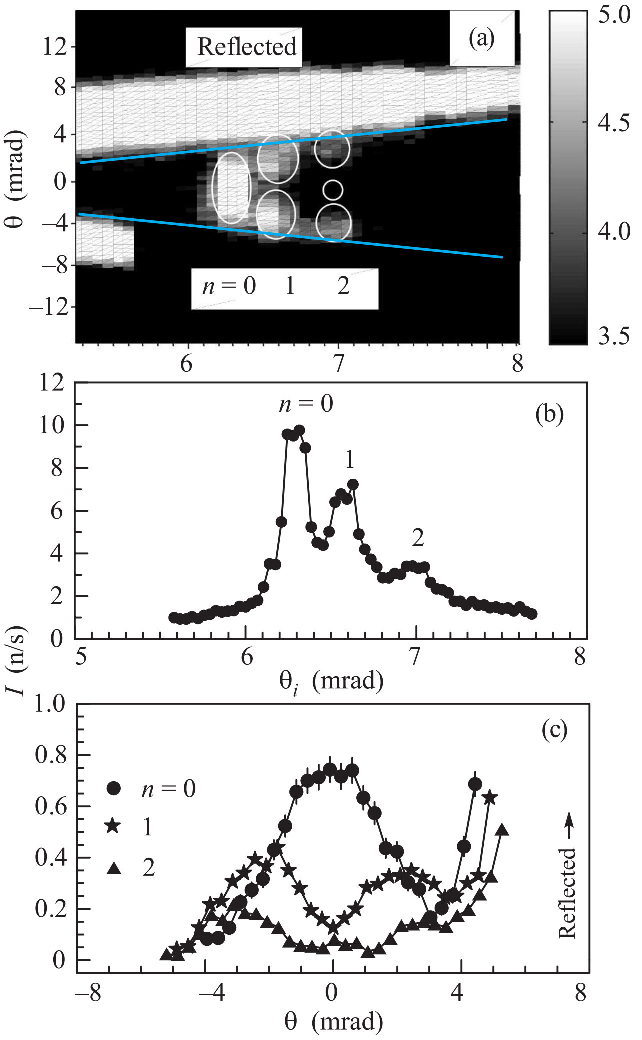


Fig. 5. The experimental data obtained for the same sample at the reflectometer NREX with the fixed neutron wavelength 4.26 Å. (a) – Two-dimensional map of the neutron intensity as a function of the incident and the final angles. (b) – The integrated microbeam intensity as a function of the grazing angle of the incident beam. (c) – The integrated microbeam intensity as a function of the angle of the scattered beam

**4. Fraunhofer diffraction.** The exit from the guiding layer is a narrow slit of the width $d = 141.7$ nm equal to the thickness of the resonant layer of the planar waveguide (Fig. 1a).

A microbeam at the slit experiences diffraction. Since it is observed by the detector at the distance $L = 4.94$ m from the slit, which is much larger than $d$, the diffraction is of the Fraunhofer type. The angular distribution $I_\theta$ of the diffracted beam is determined by the function:

$$I_\theta = I_0(\sin\beta/\beta)^2, \tag{2}$$

where $I_0$ is the intensity of the wave in the guiding layer near the exit,

$$\beta = 1/2kd\sin\theta \approx \pi d\theta/\lambda, \tag{3}$$

and $k = 2\pi/\lambda$ is the neutron wave number. The function (2) for $I_0 = 1$, $\lambda = 4.26$ Å, and $d = 141.7$ nm is shown

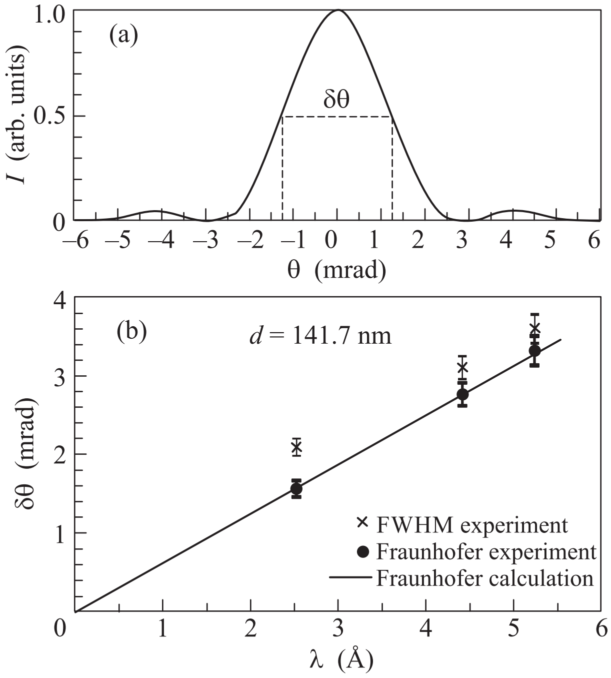


Fig. 6. (a) – Calculation of the Fraunhofer diffraction pattern for the narrow slit width $d = 141.7$ nm and the neutron wavelength 4.26 Å: the neutron intensity as a function of the final angle of diffraction. (b) – The width of the microbeam peak for the resonance $n = 0$ as a function of neutron wavelength: experimental value (open symbols); corrected experimental values (closed symbols); calculated Fraunhofer diffraction result (line)

in Fig. 6a. The full width $\delta\theta$ of the central peak at half maximum (FWHM) can be found from the equation

$$(\sin\beta/\beta)^2 = 0.5. \tag{4}$$

Graphical solution $\delta\theta = f(\lambda)$ of Eq. (4) is shown in Fig. 6b by the solid line. It follows that $\delta\theta \sim \lambda$.

For comparison with experiment we used the angular distributions obtained for resonance $n = 0$ and presented in Figs. 4a–c. We approximate the microbeam peaks by Gaussians. The widths of Gaussians increase with the neutron wavelength. In the case of the incident beam grazing angle $\theta_i = 7.68$ mrad (Fig. 4c), the form of the peak is not symmetrical. Deformation of the right side of the peak possibly can be ascribed to absorption or scattering at some defects near the exit end of the guiding film. However, the left side of the peak can be considered as non-deformed, and it is this side, which is used for definition of the Gaussian width. The experimental values of the microbeam widths (FWHM) at different neutron wavelengths are shown in Fig. 6b by open symbols. For comparison with theoretical values of the Fraunhofer diffraction $\delta\theta_{\mathrm{F}}$ it is necessary to correct the experimental data by excluding some uncertainties, as shown in the following equation

$$\delta\theta_{\mathrm{F}} = \sqrt{(\delta\theta)^2 - (\delta\theta_i)^2 - (\delta\theta_{\mathrm{det}})^2}, \tag{5}$$

where $\delta\theta_i = 1.2$ mrad is the angular divergence of the incident beam, $\delta\theta_{\mathrm{det}} = 0.55$ mrad is the angular resolution of the PSD. The corrected experimental values of the angular widths of the diffraction at the exit slit are shown in Fig. 6b by the closed symbols. They very well correlate with theoretical values, which prove that the angular width of microbeams increases with the neutron wavelength as is predicted by the theory of Fraunhofer diffraction.

**5. Discussion.** Above we reported about microbeams obtained at a pulsed reactor. Many previous experiments were performed at steady state sources. Now it is possible to discuss merits of two types of experiments with resonant planar neutron waveguides. In all the cases for production of a microbeam one needs a primary beam incident on the surface of a planar multilayer sample at some grazing angle. If the incident beam is monochromatic and well collimated, then a microbeam appears only at discrete values of the grazing angle. So it is possible: (i) to observe in one measurement a microbeam from a single resonance, and (ii) to study its angular distribution for a single wavelength. Therefore turning the multilayer sample with respect to the incident beam it is possible to study separately all the resonances and angular divergence of related microbeams. However for studying of separate resonances one needs a lot of time to get sufficiently small statistical error. Moreover, quite a good monochromatization and collimation at steady state sources are achieved with the help of Bragg reflection from single crystals. Therefore, the microbeams wavelengths are restricted to those that can be selected with single crystals. If the incident beam is not monochromatic or well collimated, then many microbeams from different resonance orders can appear. But they all overlap, and study them separately becomes impossible.

In that respect the pulsed sources with time-of-flight retlectometers have an advantage.

1. They permit to observe simultaneously all the microbeams related to different resonance orders $n = 0$, 1, 2, ... with slightly different neutron wavelengths.

2. The neutron microbeams are separated in space and time at the position of the detector.

3. The neutron wavelength in the microbeam can be varied by varying the grazing angle of the incident beam.

Another advantage of pulsed sources is a possibility to reduce a time of data acquisition because they permit to register several neutron microbeams simultaneously.

**6. Conclusion.** We have observed the system of the neutron microbeams emitted from the planar waveguide. The microbeams are produced because of resonant enhancement of the neutron wave function density inside the waveguiding layer. The microbeams angular divergence is found to coincide with that predicted by Fraunhofer diffraction theory. Experiment was carried out at the time-of-flight neutron reflectometer of the pulsed IBR-2 reactor. Several microbeams with different wavelength and space distribution were produced simultaneously and studied separately. It is a new result, which shows that microbeams can be effectively obtained at pulsed sources and used in applications. In this experiment we used nonpolarized neutrons and nonmagnetic sample. There are no limitation for production of polarized neutron microbeams, which can be used for the investigations of one-dimensional magnetic systems like magnetic microwires, domains, lithographic gratings, and vortices in superconductors.

Contrary to the fixed wavelength method at steady state sources, the time-of-flight technique allows to change the wavelength of the neutron microbeam by changing grazing angle of the incident beam. In this way one can produce microbeams with long wavelength. Here with the help of the cold neutron source we were able to produce microbeams with wavelength 5.25 Å, but there are no limitations for production of microbeams with even longer wavelength.

We thank our referee, who pointed out that a situation similar to channeling is realized in Laue diffraction in single crystals [16]. When the neutrons fell at the Bragg angle perpendicularly to the crystallographic planes the standing waves propagating along the crystallographic planes are formed. They go out from the end face of the crystal in reflected and forward directions. The direct and the diffracted beams are spatially separated from the direct beam transmitted through the crystal without diffraction. In [16] the neutron speed along diffracting crystalline planes could be order of magnitude smaller than the initial neutron speed.

The channeling phenomenon was also observed with electrons in single Si crystals in Tomsk [17]. At different angles of incidence of electrons several bound states in the transverse direction were created.

We considered channeling in a multilayer system, but we must mention that the first multilayer periodic systems were proposed for ultracold neutrons in [18], and the first interference filter containing several layers, which is the neutron analog of the Fabry-Perot interferometer, had been proposed and produced in [19].

1. F. Ott, *Focusing Optics for Neutrons*, in: *Modern Developments in X-Ray and Neutron Optics*, Springer Series in Optical Sciences (2008), v. 137. p. 113.
2. F. Pfeiffer, V. Leiner, P. Høghøj, and I. Anderson, Phys. Rev. Lett. **88**, 055507 (2002).
3. F. Pfeiffer, P. Hoghoj, I. S. Anderson, and V. Leiner, Proc. SPIE **4509**, 79 (2001).
4. S. V. Kozhevnikov, A. Rühm, F. Ott, N. K. Pleshanov, and J. Major, Physica B **406**, 2463 (2011).
5. S. V. Kozhevnikov, A. Rühm, and J. Major, Crystallography Rep. **56**, 1207 (2011).
6. S. V. Kozhevnikov, F. Ott, J. Torrejón, M. Vázquez, and A. Thiaville, Phys. Sol. State **56**, 57 (2014) [S. V. Kozhevnikov, F. Ott, J. Torrejón, M. Vázquez, and A. Thiaville, Fizika Tverdogo Tela **56**, 63 (2014).
7. F. Ott, S. Kozhevnikov, A. Thiaville, J. Torrejon, and M. Vazquez, Nucl. Instrum. and Meth. A **788**, 29 (2015).
8. P. Thibaudeau, F. Ott, A. Thiaville, V. Dubuget, and F. Duverger, Europhys. Lett. **93**, 3700 (2011).
9. V. L. Aksenov, K. N. Jernenkov, S. V. Kozhevnikov, H. Lauter, V. Lauter-Pasyuk, Yu. V. Nikitenko, and A. V. Petrenko, *JINR Communications D13-2004-47* (2004).
10. V. Ananiev, A. Belyakov, M. Bulavin, E. Kulagin, S. Kulikov, K. Mukhin, T. Petukhova, A. Sirotin, D. Shabalin, E. Shabalin, V. Shirokov, and A. Verhoglyadov, Nucl. Instrum. Meth. B **320**, 70 (2014).
11. F. Radu and V. K. Ignatovich, Physica B **292**, 160 (2000).
12. V. K. Ignatovich and F. Radu, Phys. Rev. B **64**, 205408 (2001).
13. S. V. Kozhevnikov, V. K. Ignatovich, F. Ott, A. Rühm, and J. Major, JETP **117**, 636 (2013) [S. V. Kozhevnikov, V. K. Ignatovich, F. Ott, A. Rühm, and J. Major, ZhETF **144**, 733 (2013)].
14. Yu. V. Nikitenko, V. V. Proglyado, V. L. Aksenov, J. Surf. Invest. X-ray, Synchrotron and Neutron Techniques **8**, 961 (2014) [Yu. V. Nikitenko, V. V. Pro-

glyado, and V. L. Aksenov, Poverkhnost'. Rentgenovskie, Sinkhrotronnye i Neitronnye Issledovaniya **10**, 3 (2014)].
15. S. V. Kozhevnikov, T. Keller, Yu. N. Khaydukov, F. Ott, A. Rühm, A. Thiaville, J. Torrejón, M. Vázquez, and J. Major, arXiv: 1209.3889 (2012); http://arxiv.org/abs/1209.3889.
16. V. V. Voronin, E. G. Lapin, S. Yu. Semenikhin, and V. V. Fedorov, JETP Lett. **71**, 110 (2000).
17. D. E. Popov, V. V. Kaplin, and S. A. Vorobiev, Phys. Stat. Sol. b **96**, 263 (1979).
18. A. V. Antonov, A. I. Isakov, V. I. Mikerov, and S. A. Elders, JETP Lett. **20**, 632 (1974).
19. A. A. Seregin, JETP **73**, 1634 (1977).